THE JOURNAL OF PHYSICAL CHEMISTRY C
A JOURNAL OF THE AMERICAN CHEMICAL SOCIETY

pubs.acs.org/JPCC

Article

Impact of the Environment of BEA-Type Zeolites for Sorption of Water and Cyclohexanol

Sungmin Kim, Nicholas R. Jaegers, Wenda Hu, Jian Zhi Hu, Feng Chen, Qiang Liu, Donald M. Camaioni, Miroslaw A. Derewinski, Oliver Y. Gutiérrez, Yue Liu, and Johannes A. Lercher*

Cite This: J. Phys. Chem. C 2023, 127, 23390−23399

Read Online

ACCESS | Metrics & More | Article Recommendations | Supporting Information

ABSTRACT: The (mutual) interactions of water and cyclohexanol with the pore walls and functional groups of Brønsted acidic zeolites of the BEA type (H-BEA) have been investigated. Upon reaction with Brønsted acid sites, water forms hydrated hydroxonium ions limited in size by the sorption free energy, creating in this way domains occupied by water. Organic molecules, such as cyclohexanol, occupy the remaining unoccupied volume. The pore size of the zeolite H-BEA stabilizes hydrated hydroxonium ions ($H^+(H_2O)_{10}$) that are two H_2O molecules larger than those formed in the smaller pore zeolite H-ZSM-5. Increasing the density of hydroxonium ions by increasing the concentration of aluminum in the zeolite gradually leads to less negative standard free energy of adsorbed cyclohexanol. The increasing proximity of positive charges of the hydroxonium ions induces a higher excess chemical potential of the sorbed molecule, which is manifested in a weakened interaction strength with the zeolite pores.

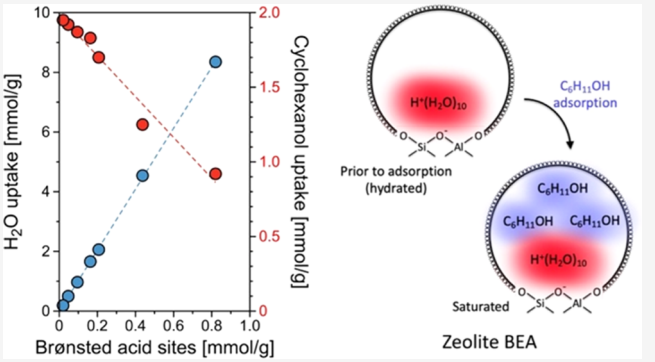

1. INTRODUCTION

Zeolites are microporous aluminosilicates widely used as sorbents and catalysts. Brønsted acid sites (BAS) are formed by protons that balance the negative charges resulting from the substitution of Si^{4+} by Al^{3+} at tetrahedral positions in the framework.[1,2] The well-defined crystallinity and near-molecular pore dimensions make zeolites highly active and selective catalysts for a variety of reactions.[3−5] Thus, understanding the interactions of molecules, such as functionalized hydrocarbons, with BAS in the confined environments of zeolite pores is important to control the physicochemical processes that govern sorption and reactivity. The heterogeneous environment of zeolite pores (silica channels with OH groups of BAS) determines the colligative properties of the zeolite, such as surface tension and wetting, and imposes complex effects on catalysis.

In aqueous environments, protons can be transferred to water molecules, forming hydroxonium ions (H_3O^+), which strongly affect sorption in the micropores.[6−8] The constraints of the pores not only influence sorption but also may stabilize charged transition states of catalyzed reactions, enhancing conversion rates compared to identical substrates and solvent compositions in mesopores or bulk solution environments.[9−11] For H-MFI, in the presence of water, hydrated hydroxonium ions consist of one hydrated proton and approximately eight water molecules, i.e., $H^+(H_2O)_8$.[6] This size is determined by the interactions with the pores, influencing the standard free energy of the hydroxonium ion.[6,12] As a result, the catalytic activity of hydroxonium ions in the constrained environment is up to 2 orders of magnitude higher than in solution.[13,14] Thus, understanding and tailoring the nature of water in zeolite pores are crucial to predict and control rates of hydroxonium ion-catalyzed reactions.

In this work, we quantitatively describe the pore environment of H-BEA to address the nature and thermodynamics of the solvation of BAS and cyclohexanol in the presence of water. We utilize a wide range of H-BEA zeolites with varying BAS concentrations, minimizing the contribution of defect sites on the sorption of water, and use the prototypical cyclohexanol sorption and dehydration to exemplify the catalytic chemistry of functionalized organic molecules under such conditions.

2. EXPERIMENTAL METHODS

2.1. Chemicals. Octadecyltrichlorosilane (Sigma-Aldrich, >90%), cyclohexanol (Sigma-Aldrich, 99%), cyclohexene (Sigma-Aldrich, 99%, GC-grade), 1,3-dimethoxy-benzene

Received: August 10, 2023
Revised: October 18, 2023
Accepted: October 24, 2023
Published: November 27, 2023

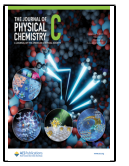

https://doi.org/10.1021/acs.jpcc.3c05405
J. Phys. Chem. C 2023, 127, 23390−23399

(Sigma-Aldrich, 99%), dichloromethane (Sigma-Aldrich, HPLC grade), tetraethylammonium hydroxide (Sigma-Aldrich, 35 wt % in H_2O), hydrofluoric acid (Sigma-Aldrich, 48 wt % in H_2O), and sodium sulfate (Acros Organics, 99%, anhydrous) were used as received without further purification.

2.2. Preparation of Low-Defect H-BEA. Low-defect H-BEA zeolite was synthesized in the presence of fluoride. The detailed procedures have been reported elsewhere.[15,16] In brief, we used a hydrothermal synthesis at 140 °C, starting with a gel molar composition of SiO_2: xAl_2O_3:(0.54 + 2x) TEAOH:(0.54 + 2x) HF:(7 + 2x) H_2O. The obtained solid was separated from the liquid by filtration and washed with deionized water until neutral pH. Afterward, it was calcined at 500 °C for 2 h in synthetic air to decompose the tetraethylammonium cation and to remove fluoride anions. Materials with different Si/Al ratios (15 to 400) were prepared by changing the gel composition.

2.3. Characterization. *2.3.1. Inductively Coupled Plasma Optical Emission Spectroscopy (ICP-OES).* The elemental compositions of the materials were determined by using a PerkinElmer 7300DV ICP-OES instrument. Prior to analysis, the H-BEA samples (50−60 mg) were digested with HNO_3 (3 mL)/HCl (2 mL)/HF (0.5 mL)/H_2O (0.5 mL) in a sealed vessel at 210 °C for 30 min. After cooling to room temperature, 1.5 mL of saturated boric acid solution was added and then heated at 180 °C for 20 min.

2.3.2. X-ray Diffraction (XRD). The diffractograms were collected using a Rigaku Mini Flex II benchtop X−ray diffractometer operated at 40 kV and 15 mA using Cu Kα radiation (0.154056 nm). Measurements were conducted on a rotating powder sample holder in the 2θ range of 5−90° with 0.02°/s step size.

2.3.3. N_2 Physisorption. The porosity of H-BEA was assessed by N_2 physisorption at −196 °C using a Micrometrics ASAP 2020. Prior to N_2 adsorption, each sample was degassed at 300 °C for 5 h under a vacuum (10^{-3} mbar). The Brunauer−Emmett−Teller, Barrett−Joyner−Halenda, and t-plot methods were employed to determine the specific surface area, mesopore volume, and micropore volume, respectively.

2.3.4. ^{27}Al MAS NMR. Ultrahigh-magnetic field ^{27}Al MAS NMR experiments were performed on a Varian-Agilent Inova 63 mm wide-bore 850 MHz NMR spectrometer. A commercial 3.2 mm pencil-type MAS probe was used, allowing for the use of typical 15 mg of sample. A single-pulse sequence with a pulse length of 0.4 μs, corresponding to a pulse angle of 45°, was selected for acquiring ^{27}Al MAS NMR spectra with a recycle time of 1 s and a total accumulation of 5000 scans. The spectra were acquired at a sample spinning rate of 20 kHz ± 2 Hz and were referenced to 1.5 M $Al(NO_3)_3$ in H_2O (0 ppm) by using the center of the octahedral peak of solid γ-Al_2O_3 (at 13.8 ppm) as a secondary reference. For quantitative measurements, the weights of samples loaded into the MAS rotor were recorded and four spectra were acquired to check the measurement stability of the spectrometer. Matching and tuning conditions of the radio frequency circuit of the NMR probe were set using a network analyzer for each sample. All other experimental conditions were kept identical for all analyzed samples. In this way, the absolute peak areas normalized to the sample mass yielded a calibration factor when being plotted against known Al concentrations derived from elemental analysis. The spectra were analyzed using NUTS NMR data processing software (Acorn NMR Inc.).

2.3.5. ^{29}Si MAS NMR. The Bloch-decay ^{29}Si MAS NMR experiments were performed by using a Varian Inova 89 mm wide−bore 300 MHz NMR spectrometer and a 5 mm HXY MAS Chemagnetics style probe. The following parameters were used: a pulse width of 0.4 μs, corresponding to a 9° tip angle, and 60 s recycle delay, ensuring the acquisition of a fully relaxed spin. The number of scans accumulated around 6000. The spinning speed was set to 5 kHz.

2.3.6. Infrared (IR) Spectroscopy. A self-supporting disc of H-BEA with a density of approximately 10 mg/cm^2 was loaded in the *in situ* IR cell. The sample disc was evacuated (10^{-7} mbar), treated to 450 °C with a heating rate of 10 °C/min, and kept for 1 h. Then, the sample was cooled to 150 °C for collection of IR spectra. The measurements were recorded on a Thermo Scientific Nicolet IR spectrometer by using a MCT detector with a resolution of 4 cm^{-1} and accumulated for 512 scans. The acid site concentrations were determined by IR spectra of pyridine adsorbed on the H-BEA samples. After equilibration with pyridine at 0.1 mbar (0.5−1.0 h) at 150 °C, the cell was outgassed under vacuum (<1 × 10^{-4} mbar). The integral area of the bands assigned to Brønsted (1565−1515 cm^{-1}) and Lewis sites (1470−1430 cm^{-1}) were employed for quantification of acid site concentration with the molar extinction coefficients of 0.73 cm/μmol and 0.96 cm/μmol for BAS and Lewis acid sites (LAS), respectively.[17−19]

2.4. Adsorption Measurement. *2.4.1. Gas-Phase Adsorption Measurements.* Gas-phase adsorption of water and cyclohexanol in H-BEA was performed by using a Seteram microbalance connected to a vacuum system and a pressure-controlled liquid-vaporizing system. In a typical experiment, 30−40 mg of H-BEA samples were loaded to the microbalance and activated under a vacuum (≈10^{-4} mbar) at 500 °C for 5 h followed by cooling to 25 °C. Water or cyclohexanol vapor was introduced stepwise to the activated materials through a dosing valve under controlled pressure. After equilibration, the adsorbed amount was quantified by the mass increase, and the released heat was monitored with the DSC signal.

2.4.2. Aqueous-Phase Adsorption Measurement. The aqueous-phase adsorption of cyclohexanol on H-BEA was carried out by immersing 30−40 mg of H-BEA in an aqueous solution of cyclohexanol at a certain concentration and stirring for at least 24 h. The zeolite was filtered from the liquid, and the residual concentration of cyclohexanol in the filtrate was measured with an Agilent 7890A GC equipped with a flame ionization detector (FID) and HP-5 column (25 m length and 0.25 μm i.d.) after extraction with dichloromethane. The quantification was done using 1,3-dimethoxy-benzene as an internal standard. The uptake was determined by the change in bulk concentration, volume of the solution, and mass of the solid sample as shown in eq 1

$$Q = Q_{sat} \cdot \frac{K_{ads}^{0}[\text{Cy-C}_6\text{OH}]_{aq}}{1 + K_{ads}^{0}[\text{Cy-C}_6\text{OH}]_{aq}} \quad (1)$$

where Q is the cyclohexanol uptake; Q_{sat} is saturation uptake of cyclohexanol; $[\text{Cy-C}_6\text{OH}]_{aq}$ is the equilibrium concentration of aqueous cyclohexanol; and K_{ads}^{0} is the adsorption constant. The coverage of cyclohexanol (θ) can be expressed by the quotient Q/Q_{sat} ($\theta = Q/Q_{sat}$).

3. RESULTS AND DISCUSSION

3.1. Physicochemical Properties of H-BEA. The crystallinity and structure of the H-BEA (Si/Al = 15−400)

https://doi.org/10.1021/acs.jpcc.3c05405
J. Phys. Chem. C 2023, 127, 23390−23399

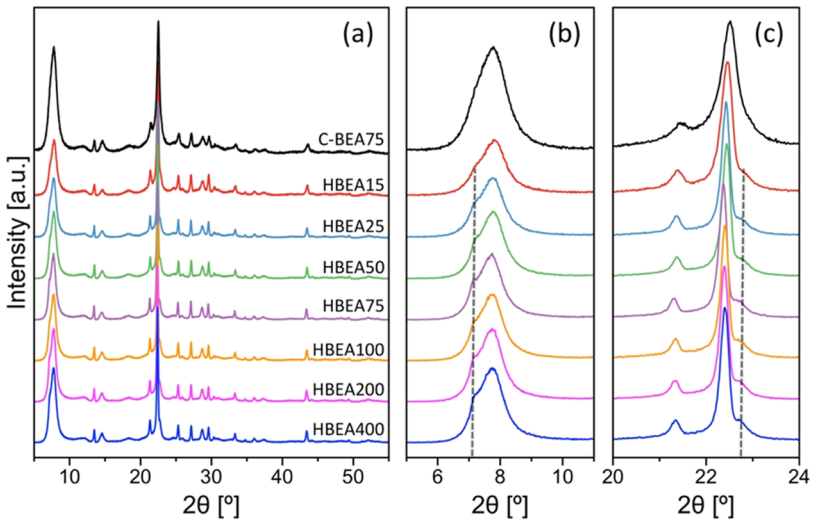

Figure 1. X-ray diffractograms of commercial H-BEA (C-BEA75) and H-BEA (Si/Al = 15−400) zeolites in the 2θ range of (a) 5−55°, (b) 5−11°, and (c) 20−24°.

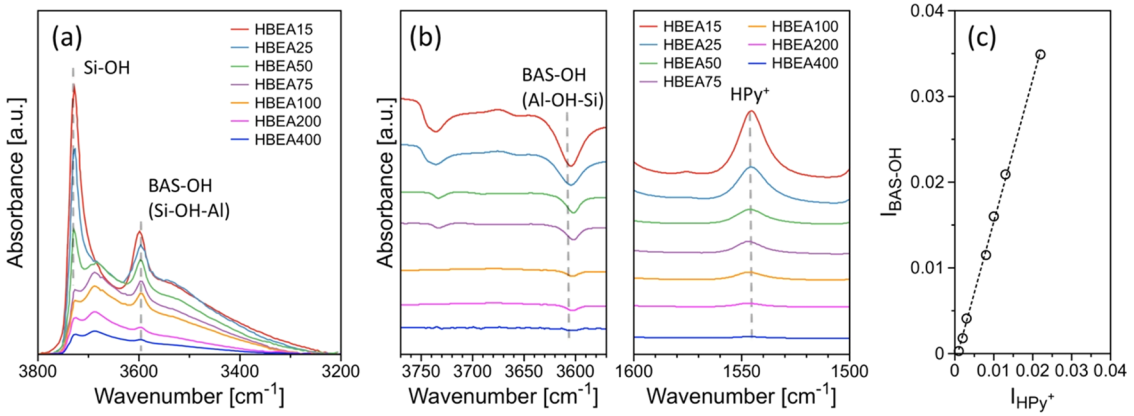

Figure 2. IR spectroscopy: (a) Hydroxyl region (3400−3800 cm^{-1}) of H-BEA at 150 °C after activation at 450 °C under a vacuum (10^{-6} mbar) for 1 h. (b) Difference IR spectra of OH^- stretching and NH^- bending vibration regions for H-BEA after pyridine adsorption (0.1 mbar) at 150 °C followed by outgassing under vacuum (10^{-6} mbar). (c) Intensity loss of the BAS−OH band at 3610 cm^{-1} (I_{BAS-OH}) after pyridine adsorption as a function of the intensity of the HPy^+ band at 1540 cm^{-1} (I_{HPy^+}). All spectra were normalized to the weight of the sample.

zeolites were characterized by XRD and compared with commercial H-BEA (Si/Al 75, denoted as C-BEA75) (Figure 1a). The diffractograms of both C-BEA75 and H-BEA zeolites indicate that they are crystalline, phase-pure, materials. Although the increase of Al in the framework may reduce the crystallinity,[20] we observed high crystallinity (>97%) in all H-BEA zeolites studied, which indicates that Al was fully incorporated in the framework. Furthermore, the signals 7.3 and 22.9° (Figure 1b,1c) are similar to those in pure silica BEA (Figure S1), indicating a low concentration of defects in the framework.[20−22] The symmetric peak at 7−8° 2θ for C-BEA75 (Figure 1b) is ascribed to polymorphs A and B,[23] which can lead to a disordered structure and some structural defects.[24] Asymmetric features in the X-ray diffractogram of H-BEA indicate an enrichment of polymorph A with relatively low structural defect sites.[20] The diffraction patterns of the studied H-BEA zeolites had a smaller full width at half maximum (fwhm) compared to C-BEA75, e.g., the peak at 22.4° is ∼2.5-fold smaller (0.16−0.19) for H-BEA zeolite than for C-BEA75 (0.43), indicating larger crystallite size for the H-BEA zeolite (Figure 1c). The growth of the BEA crystal in F^--containing medium and long aging time (20−460 h depending on the Si/Al ratio) lead to minimizing the intercrystalline growth[15,16] and few connectivity defects.[20−22]

N_2 physisorption (Table S1 and Figure S2) showed small mesopore volumes (0.05−0.08 cm^3/g) and dominant micropore volumes (0.19−0.23 cm^3/g and 0.68 nm median pore diameter) due to the minimized intercrystalline growth. In contrast, C-BEA75 had a large volume of mesopores (0.29 cm^3/g).[13]

The IR spectra of H-BEA zeolites, in the range of 3200−3800 cm^{-1}, are shown in Figure 2a. The bands at 3730−3750, 3680, and 3610 cm^{-1} are attributed to isolated Si−OH groups,[25,26] H-bonded Si−OH groups in silanol nests,[27−30] and bridging hydroxyl groups (Si−OH-Al), respectively. The latter are the strong Brønsted acid sites.[31] The isolated Si−OH groups are generated by defects in the zeolite.[16] For high-silica H-BEA zeolites (Si/Al ≥ 75), the intensity of the OH band at 3735 cm^{-1} was significantly reduced compared to low-silica materials (Si/Al < 75), indicating a decreasing concentration of defects. Higher Si/Al ratios led to a lower intensity of the bands of bridging Si−OH-Al groups at 3610 cm^{-1}, reflecting the decreasing Brønsted acid site concentration.

https://doi.org/10.1021/acs.jpcc.3c05405
J. Phys. Chem. C 2023, 127, 23390−23399

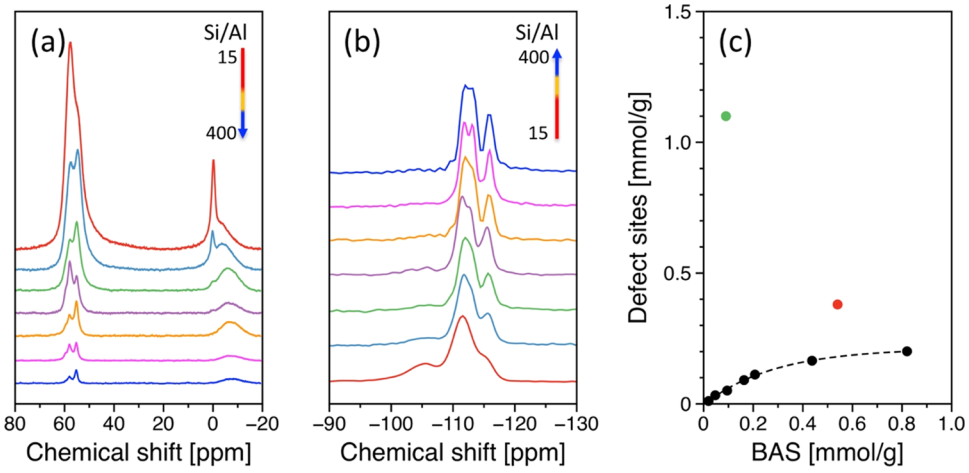

Figure 3. NMR spectroscopy: (a) ^{27}Al NMR spectra and (b) ^{29}Si NMR spectra of H-BEA zeolites (Si/Al = 15−400). (c) Defect concentration quantified by Bloch-decay ^{29}Si MAS NMR as a function of the BAS concentration. The defect sites of H-BEA (Si/Al = 15) prepared using alkaline medium (red) and defective B-BEA (green) were added for comparison.

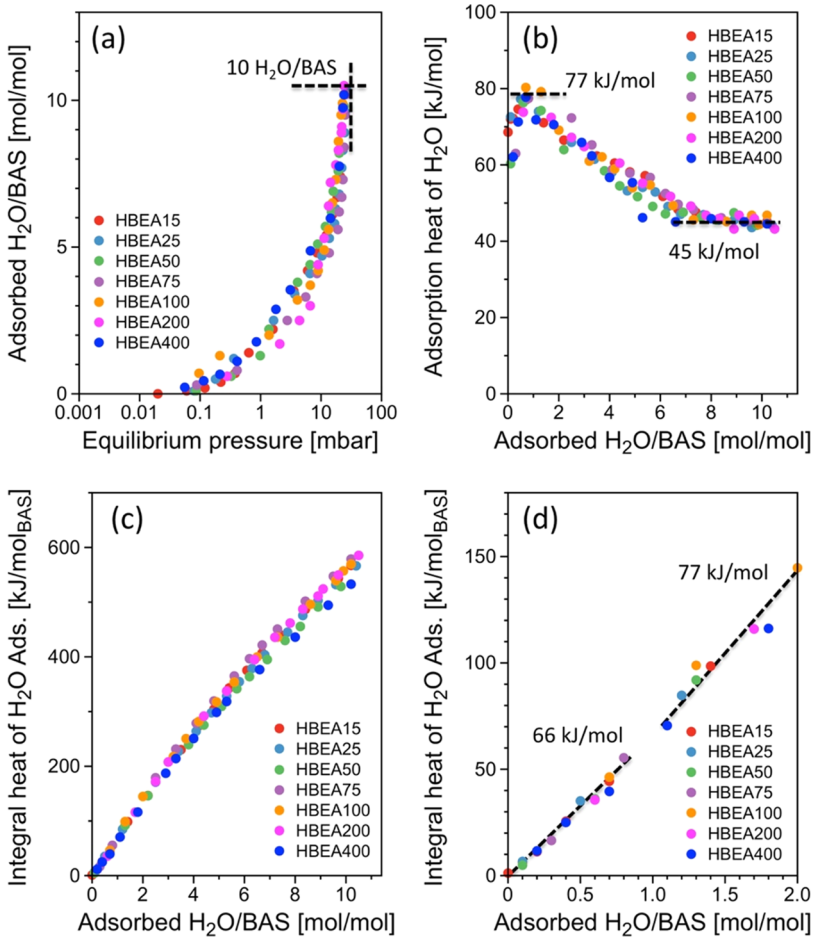

Figure 4. Gas-phase H_2O adsorption isotherm on H-BEA: (a) Adsorption isotherm and (b) heat of adsorption of water on H-BEA zeolite (Si/Al = 15−400) at 30 °C. The uptake of water is normalized to BAS sites. (c) Integral heat of water adsorption as a function of number of water molecules per BAS sites. (d) Integral heat of 1−2 water molecules adsorption on BAS sites. The dashed lines represent the differential heat of adsorption for the first and second water molecules adsorbed on BAS.

Pyridine was adsorbed on these materials and monitored by using IR spectroscopy for quantification of the acid sites on H-BEA zeolites (Table S2). Pyridinium ions (HPy^+) are formed when pyridine adsorbs on BAS (Si−OH-Al), showing a characteristic band at 1545 cm^{-1} (Figure 2b). The decreased intensity of the Si−OH-Al band (3610 cm^{-1}), i.e., BAS sites interacting with pyridine, was proportional to the increase in intensity of the HPy^+ band (1545 cm^{-1}) (Figure 2c), suggesting that pyridine adsorbs on BAS with a ratio of one pyridine per BAS site.[32]

https://doi.org/10.1021/acs.jpcc.3c05405
J. Phys. Chem. C 2023, 127, 23390−23399

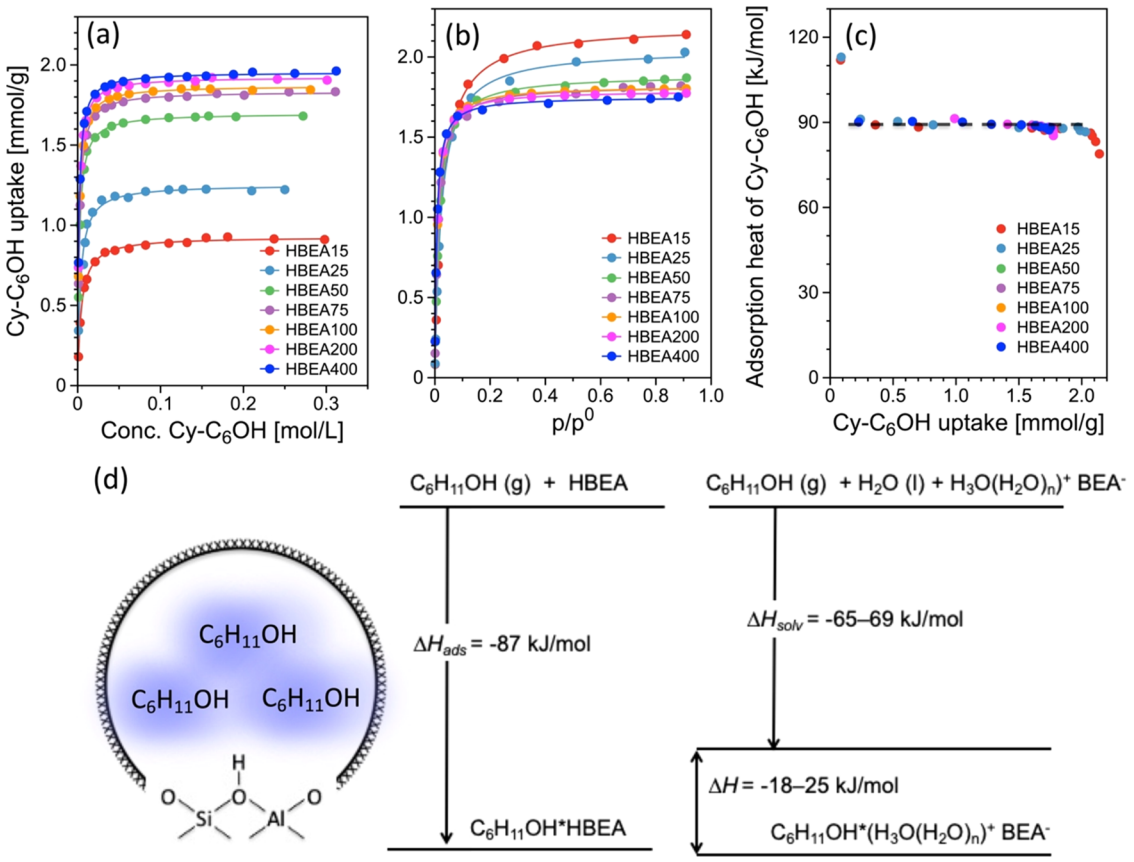

Figure 5. Cyclohexanol adsorption on H-BEA: Adsorption isotherms of (a) aqueous-phase and (b) gas-phase cyclohexanol on H-BEA zeolites (Si/Al = 15−400) at 30 °C. The solid lines represent the regression to the Langmuir isotherm model. (c) Heat of adsorption of gas-phase cyclohexanol on BEA at 30 °C, as a function of cyclohexanol uptake. (d) Born−Haber cycle of gas-phase and aqueous-phase cyclohexanol on H-BEA zeolites.

3.2. Quantification of Al Sites and Defect Sites by ^{27}Al NMR and ^{29}Si NMR. The configuration and distribution of Al sites in the H-BEA zeolites were examined by ^{27}Al MAS NMR (Figure 3a). We assumed that all Al sites can be detected by both ICP-OES and ^{27}Al MAS NMR. The total Al concentration in H-BEA was quantified by using ICP-OES (Table S1). The ratios of tetrahedral to octahedral Al sites were determined by ^{27}Al MAS NMR (Figure 3a). Tetrahedral and octahedral Al sites were, thus, quantified by the combination of ^{27}Al MAS NMR and ICP-OES. The amounts of Si or Al and the Si/Al ratios in the materials matched the nominal ratios (Table S2). Signals of tetrahedral Al sites at 54−59 ppm were observed in ^{27}Al MAS NMR, indicating different chemical environments of the 9 Al T-sites in the H-BEA framework.[33] The relatively narrow line width for tetrahedral Al sites in H-BEA zeolites with a low concentration of Al suggests that Al atoms are mostly incorporated into the framework, i.e., Al(OSi)$_4$.[34] Furthermore, the concentration of tetrahedral Al sites in H-BEA zeolites showed good agreement with the BAS concentration determined by IR spectroscopy of adsorbed pyridine, i.e., the concentration of tetrahedral Al sites and BAS increased from 18 and 20 μmol/g for HBEA400 to 806 and 820 μmol/g for HBEA15, respectively (Table S2). This indicates the absence of distorted tetrahedral Al sites.[35]

The narrow peak for octahedral Al sites in ^{27}Al MAS NMR spectra is produced by the highly symmetric coordination, which reduces its quadrupolar moment. Distorted extra-framework Al (EFAl) species lead to broad peaks at −10−5 ppm (beside the narrow peak at 0 ppm).[36] We observed the signal of symmetric EFAl sites at 0 ppm decreasing from 50 μmol/g on HBEA15 to 1 μmol/g on HBEA75 (Table S2) and becoming negligible in H-BEA with low Al contents (Si/Al ≥ 100).

For the quantification of the defect sites, Bloch-decay ^{29}Si MAS NMR was employed to characterize the Si−O−Si connectivity in the zeolite framework (Figure 3b). Q3 (−100 to −108 ppm) and Q4 (−109 to −118 ppm) sites were observed in the ^{29}Si MAS NMR spectra for H-BEA zeolites. Q4 represents Si(OSi)$_4$ sites, and Q3 sites correspond to (SiO)$_3$SiOAl or (SiO)$_3$SiOH. The signal at −103 ppm is mostly related to SiOH at defect sites. This is quantified by subtracting the Al(SiOAl) in Q3 at −106 ppm, excluding the EFAl sites quantified by ^{27}Al MAS NMR.[37,38] The defect sites for H-BEA decreased from 201 to 11 μmol/g with a decrease of BAS sites (Table S2 and Figure 3c). Nevertheless, the defect site concentrations in H-BEA zeolites are significantly lower than those in defective H-BEA synthesized in alkaline medium (380 μmol/g) and deboronated B-BEA (1110 μmol/g).[16,39,40] This finding shows that the fluoride synthesis route generates much fewer lattice defects in H-BEA than those by other methods. Nevertheless, the defect site concentration is 25−70% when compared to the BAS concentration.

3.3. Water and Cyclohexanol Adsorption on BAS. *3.3.1. Water Adsorption on BAS.* The gas-phase water uptake was reduced with decreasing BAS concentration in H-BEA (Figure S3a). However, upon normalizing the water uptake to the concentration of BAS sites (Figures 4a and S3b), 10 water molecules were consistently adsorbed per BAS site on all

https://doi.org/10.1021/acs.jpcc.3c05405
J. Phys. Chem. C 2023, 127, 23390−23399

Table 1. Adsorption Properties of Cyclohexanol on H-BEA Zeolite in Water

zeolite	BAS[a] [mmol/g]	$V_{micropore}$[b] [cm^3/g]	sat. uptake[c] [mmol/g]	adsorption constant[c]	adsorption heat[d] [kJ/mol]	I_{HBEA}[e] [mol/L]	activity coefficient	chemical potential [kJ/mol]
HBEA15	0.820	0.235	0.92	313	18.2	1.25	2.06	1.79
HBEA25	0.437	0.213	1.25	405	20.0	0.67	1.47	0.95
HBEA50	0.207	0.201	1.70	480	22.5	0.32	1.20	0.45
HBEA75	0.163	0.203	1.83	533	23.5	0.25	1.15	0.36
HBEA100	0.095	0.194	1.87	573	24.1	0.15	1.09	0.21
HBEA200	0.047	0.192	1.92	623	24.8	0.07	1.04	0.10
HBEA400	0.020	0.188	1.95	648	25.2	0.03	1.02	0.04

[a]The BAS concentrations were quantified using the molar extinction coefficients (0.73 and 0.96 cm/μmol for BAS and LAS, respectively) for the Brønsted (1565−1515 cm^{-1}) and Lewis peaks (1470−1430 cm^{-1}) normalized by the disc weight, after outgassing the physisorbed pyridine at 150 °C. [b]The pore volume in micropores was determined from N_2 physisorption using the *t*-plot method. [c]Saturated uptake and adsorption constant of aqueous-phase cyclohexanol were obtained by fitting the adsorption isotherms with the Langmuir adsorption equation. [d]The adsorption heat of aqueous-phase cyclohexanol was measured by calorimetry. [e]Ionic strength was normalized BAS to H-BEA crystalline volume.

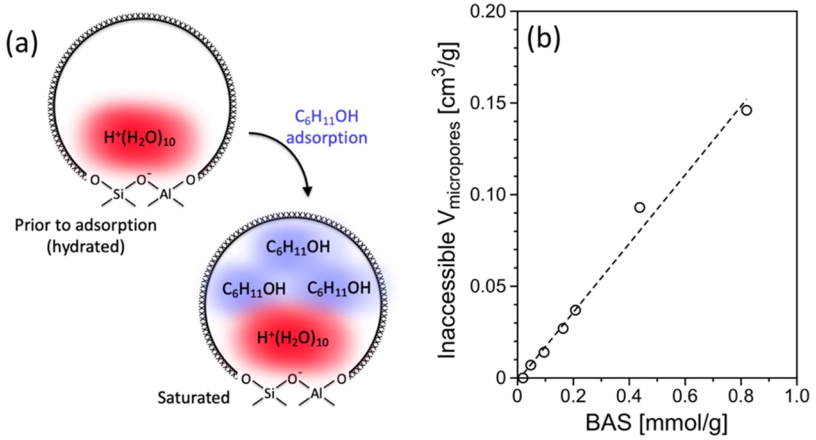

Figure 6. Water adsorption on H-BEA: (a) Scheme of micropores in the H-BEA zeolite before cyclohexanol adsorption and saturation adsorption. (b) Inaccessible micropore volume in the H-BEA zeolite (Si/Al = 15−400) at saturated cyclohexanol adsorption as a function of BAS sites.

materials, including low-defect and defective H-BEA. On the other hand, water uptake normalized by the sum of BAS and defect sites showed a lack of correlation (Figure S3c). This finding suggests that the defect sites impact drastically less the adsorption of water than BAS. The heat of water adsorption, as a function of the molecule adsorbed per BAS (Figure 4b), increased from 66 ± 7 kJ/mol for the first water molecule to 77 ± 7 kJ/mol for the second one. Increasing further the amount of adsorbed water gradually reduced the heat, reaching 45 ± 2 kJ/mol for the 10th water molecule. This trend and magnitude agree well with the adsorption heat of water on BAS of H-MFI decreasing with increasing water loadings reaching the condensation heat of water.[6,41]

The changes of adsorption heat with the number of water molecules on BAS were also observed in the integral heat of adsorption, i.e., heat of water adsorption normalized to BAS (Figure 4c). The heat of adsorption, shown in the slope of the curve, increased from 66 to 75 kJ/mol for the first and second water molecules adsorbed, respectively (Figure 4d). According to density functional theory (DFT), the first water molecule adsorbed on BAS interacts via hydrogen bonding, having a low adsorption heat, while the second water molecule induces proton transfer to water, forming the protonated bimolecular cluster $H^+(H_2O)_2$.[42,43] Additional water molecules adsorb on this hydroxonium ion core, forming the hydration shell. For the 10th water molecule per BAS, the adsorption heat was measured to be 45 kJ/mol, which is close to the condensation heat of water (41 kJ/mol) at 30 °C.[44] The adsorption heat of gas-phase water enabled us to estimate the adsorption heat from the liquid water to H-BEA via a Born−Haber cycle (Figure S4) as the difference between the adsorption heat of gas-phase water (67 kJ/mol) and the condensation heat of water (45 kJ/mol), i.e., 22 ± 3 kJ/mol. The adsorption heat of liquid water, however, is gradually reduced to zero until the 10th water molecule, thus losing the driving force for adsorption.

3.3.2. Cyclohexanol Adsorption on BAS. The uptake of cyclohexanol in H-BEA in the aqueous phase linearly increased at low concentrations (<0.01 mol/L) and reached saturation at >0.04 mol/L and inconsiderably increased up to 0.3 mol/L (Figure 5a). A Langmuir adsorption formalism fits the experiment results well (solid lines in Figure 5a). Table 1 shows that the adsorption constants and the saturation uptakes increased with decreasing BAS concentration in H-BEA. Also, the adsorption heat measured decreased from 25 to 18 kJ/mol with BAS concentration (Table 1). These findings indicate stronger adsorption and higher adsorption capacity of Cy-C_6OH on H-BEA with low hydroxonium ion concentrations.

The gas-phase cyclohexanol adsorption isotherms are shown in Figure 5b. The adsorption equilibrium constants and saturation uptakes, calculated with the Langmuir model, are listed in Table S3. The saturation uptake of cyclohexanol decreased from 2.20 to 1.75 mmol/g, with increasing Si/Al ratio from 15 to 400, whereas the adsorption constant increased from 3.3 × 10^4 to 1.2 × 10^5. At saturation, the volume of cyclohexanol in the micropores varied from 0.169

https://doi.org/10.1021/acs.jpcc.3c05405
J. Phys. Chem. C 2023, 127, 23390−23399

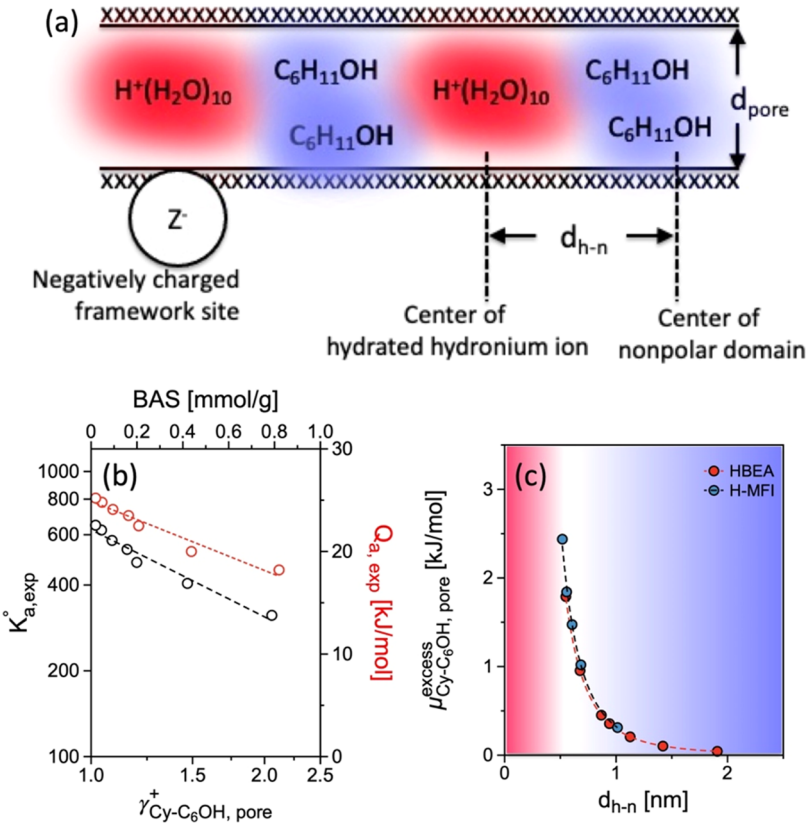

Figure 7. Adsorption properties: (a) Schematic of $H^+(H_2O)_{10}$. and nonpolar domains in H-BEA micropore channels and the distance d_{h-n} between their centers. (b) Experimentally determined equilibrium adsorption constant of aqueous cyclohexanol on BAS ($K_{a,\ exp}{}^0$) as a function of BAS and activity coefficient of aqueous cyclohexanol in the H-BEA micropore ($\gamma_{cy,\ pore}{}^+$) at room temperature. (c) Excess chemical potential ($\mu_{Cy,\ pore}{}^+$) of adsorbed cyclohexanol in the micropore of H-MFI (d_{pore} = 0.55 nm)[6] and H-BEA (d_{pore} = 0.68 nm) as a function of d_{h-n}. The d_{h-n} is half of the mean distance between two $H^+(H_2O)_{10}$. neighbors, which is estimated by the cube root of the average zeolite volume normalized to the number of $H^+(H_2O)_{10}$.

cm^3/g for HBEA400 to 0.212 cm^3/g for HBEA15 (Table S3 and Figure S5), which was close to the volume of micropores of 0.188 and 0.235 cm^3/g for HBEA400 and HBEA15, respectively. This indicates, considering the density of liquid-phase cyclohexanol (0.96 g/cm^3), that the micropores are filled with cyclohexanol under saturation. The initial heat cyclohexanol adsorption from the gas phase for HBEA15 and HBEA25 was 112 kJ/mol. This is probably due to the adsorption of cyclohexanol on the defect sites and oxide debris in the pores at very low coverage.[45−47] By establishing the adsorption of cyclohexanol on BAS, we did not consider this initial heat of adsorption. The heat of cyclohexanol adsorption from the gas phase consistently remained 87 ± 3 kJ/mol up to 2 mmol/g cyclohexanol uptake, regardless of the Si/Al ratio of H-BEA (Figure 5c). The adsorption heat of cyclohexanol in liquid water (18−25 kJ/mol, Table 1) allowed us to estimate the heat of solvation of cyclohexanol in the presence of water (65−69 kJ/mol) via the Born−Haber cycle shown in Figure 5d. The value is close to the standard solvation heat of cyclohexanol in water (≈71 kJ).[48]

Cyclohexanol completely filled the micropores of H-BEA in the gas phase (Figure S5). By considering the saturated cyclohexanol uptake in the aqueous phase even at high concentration (≈0.3 mol/L), a certain volume became inaccessible to cyclohexanol (Figures 6b and S6a). As depicted in Figure 6a, the space occupied by hydrated hydroxonium ions reduces the pore volume available for the organic substrates, e.g., phenol or cyclohexanol.[6,49] Figure 6b shows a linear correlation between inaccessible pore volume and the concentration of BAS (i.e., hydroxonium ions) in H-BEA. The hydrated hydroxonium ion concentration per H-BEA unit cell increased from 0.1 to 3.2 with increasing BAS concentration, which results in the reduction of cyclohexanol concentration from 6.8 to 3.2 molecules per unit cell (Figure S6b). Hypothesizing that the inaccessible space in micropores is occupied by hydroxonium ions, we used the slope of 187 ± 9 cm^3/mol_{BAS} to deduce a volume of 0.31 ± 0.02 nm^3 per hydroxonium ion in the micropore of the H-BEA zeolite. Assuming that H_3O^+ has the same packing density of water, this result implies that each hydroxonium ion consists of 10.4 ± 0.5 water molecules and one proton, i.e., $H^+(H_2O)_{10}$. This shows good agreement with the composition of hydroxonium ions estimated from the gas-phase adsorption of water on H-BEA, i.e., 10 water molecules and one proton.

Note that this cluster is slightly larger than that of hydrated hydroxonium ions in the zeolite H-ZSM-5, i.e., $H^+(H_2O)_8$.[6] The adsorption enthalpy and entropy of gas-phase water estimated from the adsorption constant and adsorption heat are comparable for the first water adsorption on H-MFI (−67 and −135 J/mol/K) and H-BEA (−66 and −134 J/mol/K), respectively (Table S3 and Figure S7). The protonation to the bimolecular cluster ($H^+(H_2O)_2$) leads to significantly lower adsorption enthalpies and entropies by −8 and −45 J/mol/K for H-MFI and −11 and −47 J/mol/K for H-BEA,

https://doi.org/10.1021/acs.jpcc.3c05405
J. Phys. Chem. C 2023, 127, 23390−23399

respectively. Hydration shell formation with further water addition gradually increases adsorption enthalpy and entropy (Figure S7a,b), where H-BEA shows a lower adsorption enthalpy (by 3−4 kJ/mol) and higher adsorption entropy (by 1−7 J/mol/K) until the seventh water molecule compared to H-MFI. The correlation of adsorption entropy with adsorption enthalpy (Figure S8) shows less adsorption entropy loss in H-BEA than in H-MFI, which we associate with the differences in the hydration shell in H-MFI and H-BEA. The changes of adsorption enthalpy and entropy with pore size observed in the liquid phase are consistent with those observed in the gas phase (Figure S7c,d). Therefore, the larger hydroxonium ions in H-BEA are caused by a slightly higher adsorption enthalpy of water and the lower entropy loss in the pores for H-BEA (0.67 nm) compared to H-MFI (0.55 nm).[6,12,50]

3.4. Chemical Environment in the Micropore of H-BEA in Water. In the presence of water, the hydroxonium ions formed by BAS lead to fluxional domains in the micropores of H-BEA, while the remainder are typically called a hydrophobic domain. Water is largely confined in these hydrophilic domains around the BAS (Figure 7a), but it is able to rapidly diffuse between clusters. Very high pressure (>1000 bar), however, is required for water to completely fill the pores of the siliceous zeolite.[51,52] While the hydrophobic domains are easily occupied by organic substrates, such as cyclohexanol, these molecules cannot replace water in the hydrated hydroxonium ions. Thus, domains of cyclohexanol and hydroxonium ions coexist in the micropores of H-BEA under saturation.

We have reported that the negatively charged framework sites (anions) and hydroxonium ions (cations) in the micropores of zeolites provide a quasi-solid electrolyte environment.[6] As a consequence, these cations and anions yield a specific ionic strength, making an organic substrate behave nonideally in the micropores. We calculated the ionic strength in the micropores of BEA (I_{HBEA}) using the concentrations of hydroxonium ions ($[H^+(H_2O)_{10}]$) and the negative charged framework sites ($[Z^-]$) per unit volume in H-BEA as follows

$$I_{HBEA} = 1/2[H^+(H_2O)_{10}] + 1/2[Z^-] = [H^+(H_2O)_{10}] \quad (2)$$

Hence, I_{HBEA} is proportional to the BAS concentration, which increased from 0.03 mol/L for HBEA400 to 1.25 mol/L for HBEA15 (Table 1). We used the salting-out model[6] to quantify the activity of adsorbed cyclohexanol, according to eq 3

$$\log_{10}\left(\gamma^+_{Cy\text{-}C_6OH,pore}\right) = K_s I_{HBEA} = K_s[H^+(H_2O)_{10}] \quad (3)$$

where K_s is the Setschenow constant. The adsorption constant ($K_{a,exp}{}^0$) and adsorption heat ($Q_{a,exp}$) can be further expressed as shown in eqs 4 and 5, respectively

$$\frac{\partial \log_{10}\left(K^0_{a,exp}\right)}{\partial[H^+(H_2O)_{10}]} = -K_s \quad (4)$$

$$\frac{\partial Q_{a,exp}}{\partial[H^+(H_2O)_{10}]} = 2.303RT^2\frac{\partial K_s}{\partial T} \quad (5)$$

These equations feature an exponential decrease of $K_{a,exp}{}^0$ and linear change of $Q_{a,exp}$ with the change in the concentration of hydroxonium ions ($[H^+(H_2O)_{10}]$). This is in line with the correlations observed between the adsorption constant and adsorption heat as a function of BAS concentration (Figure 7b). The regression of the experimental data using eq 4 yields a value for K_s of 0.25 ± 0.2. The activity coefficient ($\gamma^+_{Cy\text{-}C_6OH,pore}$) was then calculated using K_s and the concentration of hydroxonium ions as presented in Table 1. The activity coefficient increased with BAS concentration from 1.02 (i.e., behaving nearly ideal) on HBEA400 to 2.06 on HBEA15, which indicates an increasing deviation from ideality with increasing BAS concentrations. The activity coefficient ($\gamma > 1$) indicates a destabilization of adsorbed cyclohexanol in the micropore of H-BEA zeolite due to the presence of hydroxonium ions.

The excess chemical potential of cyclohexanol ($\mu^{excess}_{Cy\text{-}C_6OH}$) induced by the interaction with the ions can be estimated (Table 1) by using eq 6

$$\mu^{excess}_{Cy\text{-}C_6OH} = RT \ln \gamma^+_{Cy\text{-}C_6OH} \quad (6)$$

Figure 7c shows the excess chemical potential of adsorbed cyclohexanol in H-BEA as a function of the distance from the center of the hydroxonium ion to the center of the nonpolar domain (d_{h-n}). The excess chemical potential is small when d_{h-n} is larger than 1.0 nm but sharply increases at $d_{h-n} < 1.0$ nm.

Interestingly, hydroxonium ions impose a relatively lower excess chemical potential over cyclohexanol in H-BEA (1.8 kJ/mol) than in H-MFI (2.4 kJ/mol) at the same 0.5 nm d_{h-n}. This is linked to the lower adsorption heat of cyclohexanol on H-BEA (18−25 kJ/mol) compared to that of H-MFI (24−34 kJ/mol) in aqueous solution. Cyclohexanol is destabilized by the specific ionic strength in the zeolite micropore. The positive excess chemical potential of adsorbed cyclohexanol (0.1−1.8 kJ/mol for H-BEA and 0.3−2.4 kJ/mol for H-MFI) increases the standard free energy of the initial state of reacting cyclohexanol.[53] It is interesting to explore whether and how this contributes to the catalytic conversion of cyclohexanol.

4. CONCLUSIONS

The adsorption of water and cyclohexanol was studied for low-defect H-BEA zeolites prepared via the fluoride route. In the presence of water, hydrated hydroxonium ions form on Brønsted acid sites (BAS) by protonation of water, leading to localized domains next to "empty" domains in the pores. In the micropores of H-BEA, the hydrated hydroxonium ion is composed of 10 water molecules and one proton, i.e., $H^+(H_2O)_{10}$. The increase of the hydroxonium ion concentration restricts the volume of empty domains, thus reducing the adsorption capacity for cyclohexanol.

The size of the hydroxonium ions in H-BEA was about 20% larger than that in H-MFI ($H^+(H_2O)_8$). This difference results from the lower entropy loss in the larger H-BEA pore compared to H-MFI by 3−4 J/mol/K. In both cases, the "quasi-solid electrolyte" environment imposed by hydroxonium ions and the negatively charged framework induce a direct relation between the ionic strength and the excess chemical potential of the sorbed substrate. Adsorbed cyclohexanol is destabilized by its increasing excess chemical potential induced by the hydroxonium ions to a larger extent in H-MFI (0.3−2.4 kJ/mol) than in H-BEA (0.1−1.8 kJ/mol). We conclude that this weaker effect of the impact of increasing charge is related to the better shielding of the positive charge by the slightly larger hydrated hydroxonium ion. It is

https://doi.org/10.1021/acs.jpcc.3c05405
J. Phys. Chem. C 2023, 127, 23390−23399

somewhat surprising that such a small increase together with the slightly lower entropy loss of sorbed molecules in large pore zeolites such as BEA causes this measurable difference. It will be interesting to see whether or not these subtle differences induce differences in Brønsted acid-catalyzed reactions.[13]

■ ASSOCIATED CONTENT

Supporting Information

The Supporting Information is available free of charge at https://pubs.acs.org/doi/10.1021/acs.jpcc.3c05405.

Deviation of chemical potential calculation, physicochemical properties of H-BEA, adsorption free energies, enthalpies and entropies of H-BEA and H-MFI, and Born−Haber cycle of gas- and liquid-phase water adsorption on H-BEA (PDF)

■ AUTHOR INFORMATION

Corresponding Author

Johannes A. Lercher − *Institute for Integrated Catalysis and Physical Science Division, Pacific Northwest National Laboratory, Richland, Washington 99354, United States; Department of Chemistry and Catalysis Research Institute, TU München, 85748 Garching, Germany;* orcid.org/0000-0002-2495-1404; Email: Johannes.Lercher@pnnl.gov

Authors

Sungmin Kim − *Institute for Integrated Catalysis and Physical Science Division, Pacific Northwest National Laboratory, Richland, Washington 99354, United States;* orcid.org/0000-0001-6602-1320

Nicholas R. Jaegers − *Institute for Integrated Catalysis and Physical Science Division, Pacific Northwest National Laboratory, Richland, Washington 99354, United States;* orcid.org/0000-0002-9930-7672

Wenda Hu − *Institute for Integrated Catalysis and Physical Science Division, Pacific Northwest National Laboratory, Richland, Washington 99354, United States; Voiland School of Chemical Engineering and Bioengineering, Washington State University, Pullman, Washington 99163, United States*

Jian Zhi Hu − *Institute for Integrated Catalysis and Physical Science Division, Pacific Northwest National Laboratory, Richland, Washington 99354, United States;* orcid.org/0000-0001-8879-747X

Feng Chen − *Institute for Integrated Catalysis and Physical Science Division, Pacific Northwest National Laboratory, Richland, Washington 99354, United States; Gene and Linda Voiland School of Chemical Engineering and Bioengineering, Washington State University, Pullman, Washington WA 99164, United States;* orcid.org/0000-0002-5227-6119

Qiang Liu − *Department of Chemistry and Catalysis Research Institute, TU München, 85748 Garching, Germany*

Donald M. Camaioni − *Institute for Integrated Catalysis and Physical Science Division, Pacific Northwest National Laboratory, Richland, Washington 99354, United States;* orcid.org/0000-0002-2213-0960

Miroslaw A. Derewinski − *Institute for Integrated Catalysis and Physical Science Division, Pacific Northwest National Laboratory, Richland, Washington 99354, United States; Jerzy Haber Institute of Catalysis and Surface Chemistry, Polish Academy of Sciences, 30-239 Cracow, Poland;* orcid.org/0000-0003-1738-2247

Oliver Y. Gutiérrez − *Institute for Integrated Catalysis and Physical Science Division, Pacific Northwest National Laboratory, Richland, Washington 99354, United States;* orcid.org/0000-0001-9163-4786

Yue Liu − *Department of Chemistry and Catalysis Research Institute, TU München, 85748 Garching, Germany;* orcid.org/0000-0001-8939-0233

Complete contact information is available at: https://pubs.acs.org/10.1021/acs.jpcc.3c05405

Notes

The authors declare no competing financial interest.

■ ACKNOWLEDGMENTS

This work was supported by the U.S. Department of Energy (DOE), Office of Science, Office of Basic Energy Sciences (BES), Division of Chemical Sciences, Geosciences and Biosciences (impact of catalytically active centers and their environment on rates and thermodynamic states along reaction paths, FWP 47319).

■ REFERENCES

(1) Corma, A. Inorganic Solid Acids and Their Use in Acid-Catalyzed Hydrocarbon Reactions. *Chem. Rev.* **1995**, *95* (3), 559−614.

(2) Corma, A. From Microporous to Mesoporous Molecular Sieve Materials and Their Use in Catalysis. *Chem. Rev.* **1997**, *97* (6), 2373−2420.

(3) Zhao, C.; Camaioni, D. M.; Lercher, J. A. Selective catalytic hydroalkylation and deoxygenation of substituted phenols to bicycloalkanes. *J. Catal.* **2012**, *288*, 92−103.

(4) Jacobs, P. A.; Dusselier, M.; Sels, B. F. Will Zeolite-Based Catalysis be as Relevant in Future Biorefineries as in Crude Oil Refineries? *Angew. Chem., Int. Ed.* **2014**, *53* (33), 8621−8626.

(5) Zhao, C.; Lercher, J. A. Upgrading Pyrolysis Oil over Ni/HZSM-5 by Cascade Reactions. *Angew. Chem., Int. Ed.* **2012**, *51* (24), 5935−5940.

(6) Eckstein, S.; Hintermeier, P. H.; Zhao, R.; Baráth, E.; Shi, H.; Liu, Y.; Lercher, J. A. Influence of Hydronium Ions in Zeolites on Sorption. *Angew. Chem., Int. Ed.* **2019**, *58* (11), 3450−3455.

(7) Gounder, R.; Iglesia, E. The Roles of Entropy and Enthalpy in Stabilizing Ion-Pairs at Transition States in Zeolite Acid Catalysis. *Acc. Chem. Res.* **2012**, *45* (2), 229−238.

(8) Li, G.; Pidko, E. A. The Nature and Catalytic Function of Cation Sites in Zeolites: a Computational Perspective. *ChemCatChem* **2019**, *11* (1), 134−156.

(9) Zicovich-Wilson, C. M.; Corma, A.; Viruela, P. Electronic Confinement of Molecules in Microscopic Pores. A New Concept Which Contributes to the Explanation of the Catalytic Activity of Zeolites. *J. Phys. Chem. A* **1994**, *98* (42), 10863−10870.

(10) Gounder, R.; Iglesia, E. Catalytic Consequences of Spatial Constraints and Acid Site Location for Monomolecular Alkane Activation on Zeolites. *J. Am. Chem. Soc.* **2009**, *131* (5), 1958−1971.

(11) Gounder, R.; Iglesia, E. The catalytic diversity of zeolites: confinement and solvation effects within voids of molecular dimensions. *Chem. Commun.* **2013**, *49* (34), 3491−3509.

(12) Wang, M.; Jaegers, N. R.; Lee, M.-S.; Wan, C.; Hu, J. Z.; Shi, H.; Mei, D.; Burton, S. D.; Camaioni, D. M.; Gutiérrsez, O. Y.; et al. Genesis and Stability of Hydronium Ions in Zeolite Channels. *J. Am. Chem. Soc.* **2019**, *141* (8), 3444−3455.

(13) Shi, H.; Eckstein, S.; Vjunov, A.; Camaioni, D. M.; Lercher, J. A. Tailoring nanoscopic confines to maximize catalytic activity of hydronium ions. *Nat. Commun.* **2017**, *8* (1), No. 15442.

(14) Liu, Y.; Vjunov, A.; Shi, H.; Eckstein, S.; Camaioni, D. M.; Mei, D.; Baráth, E.; Lercher, J. A. Enhancing the catalytic activity of hydronium ions through constrained environments. *Nat. Commun.* **2017**, *8* (1), No. 14113.
(15) Prodinger, S.; Shi, H.; Wang, H.; Derewinski, M. A.; Lercher, J. A. Impact of structural defects and hydronium ion concentration on the stability of zeolite BEA in aqueous phase. *Appl. Catal., B* **2018**, *237*, 996−1002.
(16) Prodinger, S.; Shi, H.; Eckstein, S.; Hu, J. Z.; Olarte, M. V.; Camaioni, D. M.; Derewinski, M. A.; Lercher, J. A. Stability of Zeolites in Aqueous Phase Reactions. *Chem. Mater.* **2017**, *29* (17), 7255−7262.
(17) Emeis, C. A. Determination of Integrated Molar Extinction Coefficients for Infrared Absorption Bands of Pyridine Adsorbed on Solid Acid Catalysts. *J. Catal.* **1993**, *141* (2), 347−354.
(18) Vimont, A.; Thibault-Starzyk, F.; Daturi, M. Analysing and understanding the active site by IR spectroscopy. *Chem. Soc. Rev.* **2010**, *39* (12), 4928−4950.
(19) Lercher, J. A.; Gründling, C.; Eder-Mirth, G. Infrared studies of the surface acidity of oxides and zeolites using adsorbed probe molecules. *Catal. Today* **1996**, *27* (3), 353−376.
(20) Camblor, M. A.; Corma, A.; Valencia, S. Synthesis in fluoride media and characterisation of aluminosilicate zeolite beta. *J. Mater. Chem.* **1998**, *8* (9), 2137−2145.
(21) Camblor, M. A.; Corma, A.; Valencia, S. Spontaneous nucleation and growth of pure silica zeolite-β free of connectivity defects. *Chem. Commun.* **1996**, *20*, 2365−2366.
(22) Corma, A.; Moliner, M.; Cantín, Á.; Díaz-Cabañas, M. J.; Jordá, J. L.; Zhang, D.; Sun, J.; Jansson, K.; Hovmöller, S.; Zou, X. Synthesis and Structure of Polymorph B of Zeolite Beta. *Chem. Mater.* **2008**, *20* (9), 3218−3223.
(23) Wright, P. A.; Zhou, W.; Pérez-Pariente, J.; Arranz, M. Direct Observation of Growth Defects in Zeolite Beta. *J. Am. Chem. Soc.* **2005**, *127* (2), 494−495.
(24) Newsam, J. M.; Treacy, M. M.; Koetsier, W. T.; Gruyter, C. B. d. Structural characterization of zeolite beta. *Proc. R. Soc. Lond. A* **1988**, *420* (1859), 375−405.
(25) Maier, S. M.; Jentys, A.; Lercher, J. A. Steaming of Zeolite BEA and Its Effect on Acidity: A Comparative NMR and IR Spectroscopic Study. *J. Phys. Chem. C* **2011**, *115* (16), 8005−8013.
(26) Woolery, G. L.; Alemany, L. B.; Dessau, R. M.; Chester, A. W. Spectroscopic evidence for the presence of internal silanols in highly siliceous ZSM-5. *Zeolites* **1986**, *6* (1), 14−16.
(27) Krijnen, S.; Harmsen, R.; Abbenhuis, H.; Van Hooff, J.; Van Santen, R. Incompletely condensed silasesquioxanes as models for zeolite defect sites: an FTIR and density functional study. *Chem. Commun.* **1999**, *6*, 501−502.
(28) Kraushaar, B.; Van De Ven, L. J. M.; De Haan, J. W.; Van Hooff, J. H. C. Clusters of Terminal Groups in ZSM-5: A Study Performed by Silylation and ^{29}Si CP MAS NMR. In *Studies in Surface Science and Catalysis*; Grobet, P. J.; Mortier, W. J.; Vansant, E. F.; Schulz-Ekloff, G., Eds.; Elsevier, 1988; Vol. *37*, pp 167−174.
(29) Holm, M. S.; Svelle, S.; Joensen, F.; Beato, P.; Christensen, C. H.; Bordiga, S.; Bjørgen, M. Assessing the acid properties of desilicated ZSM-5 by FTIR using CO and 2,4,6-trimethylpyridine (collidine) as molecular probes. *Appl. Catal., A* **2009**, *356* (1), 23−30.
(30) Takei, T.; Kato, K.; Meguro, A.; Chikazawa, M. Infrared spectra of geminal and novel triple hydroxyl groups on silica surface. *Colloids Surf., A* **1999**, *150* (1), 77−84.
(31) Guisnet, M.; Ayrault, P.; Coutanceau, C.; Fernanda Alvarez, M.; Datka, J. Acid properties of dealuminated beta zeolites studied by IR spectroscopy. *J. Chem. Soc., Faraday Trans.* **1997**, *93* (8), 1661−1665.
(32) Parrillo, D. J.; Adamo, A. T.; Kokotailo, G. T.; Gorte, R. J. Amine adsorption in H-ZSM-5. *Appl. Catal.* **1990**, *67* (1), 107−118.
(33) Vjunov, A.; Fulton, J. L.; Huthwelker, T.; Pin, S.; Mei, D.; Schenter, G. K.; Govind, N.; Camaioni, D. M.; Hu, J. Z.; Lercher, J. A. Quantitatively Probing the Al Distribution in Zeolites. *J. Am. Chem. Soc.* **2014**, *136* (23), 8296−8306.
(34) Shi, J.; Anderson, M. W.; Carr, S. W. Direct Observation of Zeolite A Synthesis by in Situ Solid-State NMR. *Chem. Mater.* **1996**, *8* (2), 369−375.
(35) Gounder, R.; Jones, A. J.; Carr, R. T.; Iglesia, E. Solvation and acid strength effects on catalysis by faujasite zeolites. *J. Catal.* **2012**, *286*, 214−223.
(36) Beers, A. E. W.; van Bokhoven, J. A.; de Lathouder, K. M.; Kapteijn, F.; Moulijn, J. A. Optimization of zeolite Beta by steaming and acid leaching for the acylation of anisole with octanoic acid: a structure−activity relation. *J. Catal.* **2003**, *218* (2), 239−248.
(37) Müller, M.; Harvey, G.; Prins, R. Quantitative multinuclear MAS NMR studies of zeolites. *Microporous Mesoporous Mater.* **2000**, *34* (3), 281−290.
(38) Engelhardt, G.; Michel, D. *High-Resolution Solid-State NMR of Silicates and Zeolites* US DOE; 1987.
(39) Derewinski, M.; Renzo, F. D.; Espiau, P.; Fajula, F.; Nicolle, M.-A. Synthesis of Zeolite Beta in Boron-Aluminium Media. In *Studies in Surface Science and Catalysis*; Jacobs, P. A.; Jaeger, N. I.; Kubelková, L.; Wichterlov′, B., Eds.; Elsevier, 1991; Vol. *69*, pp 127−134.
(40) Prodinger, S.; Derewinski, M. A.; Vjunov, A.; Burton, S. D.; Arslan, I.; Lercher, J. A. Improving Stability of Zeolites in Aqueous Phase via Selective Removal of Structural Defects. *J. Am. Chem. Soc.* **2016**, *138* (13), 4408−4415.
(41) Olson, D. H.; Haag, W. O.; Borghard, W. S. Use of water as a probe of zeolitic properties: interaction of water with HZSM-5. *Microporous Mesoporous Mater.* **2000**, *35*−*36*, 435−446.
(42) Bordiga, S.; Regli, L.; Lamberti, C.; Zecchina, A.; Bjørgen, M.; Lillerud, K. P. FTIR Adsorption Studies of H_2O and CH_3OH in the Isostructural H-SSZ-13 and H-SAPO-34: Formation of H-Bonded Adducts and Protonated Clusters. *J. Phys. Chem. B* **2005**, *109* (16), 7724−7732.
(43) Mei, D.; Lercher, J. A. Mechanistic insights into aqueous phase propanol dehydration in H-ZSM-5 zeolite. *AIChE J.* **2017**, *63* (1), 172−184.
(44) Joshi, K. L.; Psofogiannakis, G.; van Duin, A. C. T.; Raman, S. Reactive molecular simulations of protonation of water clusters and depletion of acidity in H-ZSM-5 zeolite. *Phys. Chem. Chem. Phys.* **2014**, *16* (34), 18433−18441.
(45) Lee, C. C.; Gorte, R. J.; Farneth, W. E. Calorimetric Study of Alcohol and Nitrile Adsorption Complexes in H-ZSM-5. *J. Phys. Chem. B* **1997**, *101* (19), 3811−3817.
(46) Thamm, H. Calorimetric study on the state of C1−C4 alcohols sorbed on silicalite. *J. Chem. Soc., Faraday Trans. 1* **1989**, *85* (1), 1−9.
(47) Zhi, Y.; Shi, H.; Mu, L.; Liu, Y.; Mei, D.; Camaioni, D. M.; Lercher, J. A. Dehydration Pathways of 1-Propanol on HZSM-5 in the Presence and Absence of Water. *J. Am. Chem. Soc.* **2015**, *137* (50), 15781−15794.
(48) Costa, F. S.; Eusébio, M. E.; Redinha, J. S.; Luísa, P.; Leitão, M. Enthalpies of solvation of hydroxyl cyclohexane derivatives in different solvents. *J. Chem. Thermodyn.* **1999**, *31* (7), 895−903.
(49) Eckstein, S.; Hintermeier, P. H.; Olarte, M. V.; Liu, Y.; Baráth, E.; Lercher, J. A. Elementary steps and reaction pathways in the aqueous phase alkylation of phenol with ethanol. *J. Catal.* **2017**, *352*, 329−336.
(50) Grifoni, E.; Piccini, G.; Lercher, J. A.; Glezakou, V.-A.; Rousseau, R.; Parrinello, M. Confinement effects and acid strength in zeolites. *Nat. Commun.* **2021**, *12* (1), 2630.
(51) Karbowiak, T.; Saada, M.-A.; Rigolet, S.; Ballandras, A.; Weber, G.; Bezverkhyy, I.; Soulard, M.; Patarin, J.; Bellat, J.-P. New insights in the formation of silanol defects in silicalite-1 by water intrusion under high pressure. *Phys. Chem. Chem. Phys.* **2010**, *12* (37), 11454−11466.
(52) Humplik, T.; Raj, R.; Maroo, S. C.; Laoui, T.; Wang, E. N. Effect of Hydrophilic Defects on Water Transport in MFI Zeolites. *Langmuir* **2014**, *30* (22), 6446−6453.
(53) Pfriem, N.; Hintermeier, P. H.; Eckstein, S.; Kim, S.; Liu, Q.; Shi, H.; Milakovic, L.; Liu, Y.; Haller, G. L.; Baráth, E. Role of the ionic environment in enhancing the activity of reacting molecules in zeolite pores. *Science* **2021**, *372* (6545), 952−957, DOI: 10.1126/science.abh3418.

https://doi.org/10.1021/acs.jpcc.3c05405
J. Phys. Chem. C 2023, 127, 23390−23399